Cite this: *Soft Matter*, 2012, **8**, 797

www.rsc.org/softmatter

PAPER

Structure and dynamics of balanced supercritical CO_2-microemulsions

Michael Klostermann,[a] Reinhard Strey,[a] Thomas Sottmann,*[a] Ralf Schweins,[b] Peter Lindner,[b] Olaf Holderer,*[c] Michael Monkenbusch[d] and Dieter Richter[d]

Received 10th August 2011, Accepted 19th October 2011
DOI: 10.1039/c1sm06533e

Balanced $scCO_2$-microemulsions contain equal volumes of water and CO_2 and are a novel class of microemulsions of substantial interest for both fundamental research and technical applications. One existing feature of these systems is that the solvent quality of $scCO_2$, and hence the overall microemulsion properties, is tuned simply by adjusting pressure, which is not possible with "classical" microemulsions containing oil instead of CO_2. Motivated by this, we systematically investigated the phase behavior, the microstructure, and the dynamics of balanced microemulsion systems of the type H_2O–CO_2–Zonyl FSO 100/Zonyl FSN 100. In systematic phase behavior studies, we found that upon increasing pressure, CO_2 and water are more efficiently solubilized. Small angle neutron scattering (SANS) experiments were conducted in order to determine the topology and the length scales of the underlying microstructure. The results obtained strongly suggest the existence of bicontinuously structured microemulsions with an adjustable characteristic length scale of up to 330 Å. From a quantitative analysis of the SANS data, we found that at a fixed microemulsion composition the stiffness of the surfactant membrane is increased solely by increasing the pressure, whereby the renormalization corrected (*i.e.* bare) bending rigidity $\kappa_{0,SANS}$ rises from $\kappa_{0,SANS} = 0.88\ k_BT$ at 200 bar to $0.93\ k_BT$ at 300 bar. These findings were confirmed with high pressure neutron spin echo experiments.

1 Introduction

Mixtures of water, oil and surfactants can form thermodynamically stable microemulsions which are macroscopically homogeneous and isotropic but nanoscopically structured (length scale 1–100 nm) mixtures. Depending on the composition and the temperature, a variety of different structures can be found in which water and oil domains are separated by a surfactant monolayer. If equal volumes of water and oil are present, bicontinuous structures are formed at certain temperatures and surfactant concentrations.[1–3]

In the last few decades considerable effort has been invested in the theoretical description of bicontinuous microemulsions whereas different models have been used, *e.g.* microscopic lattice models, phenomenological Ginzburg–Landau approaches or membrane theories.[4] In the latter case theoretical descriptions are based on the elastic bending energy[5] of the surfactant layer:

$$F_{el} = \int \left[\frac{k}{2} (c_1 + c_2 - 2c_0)^2 + \bar{\kappa} c_1 c_2 \right] dS, \quad (1)$$

Here κ is the bending rigidity, $\bar{\kappa}$ is the saddle splay modulus, c_0 is the spontaneous curvature and $c_i = 1/R_i$ is the principle curvatures with the principle curvature radii R_i. The bending rigidity defines the energy cost of deformations of the membrane, while the saddle splay modulus is related to the energy cost of changes of topological connectivity. The effect of thermal fluctuations of the amphiphilic film which lead to a softening of membranes can be incorporated by replacing the elastic moduli in eqn (1) with their renormalized, scale dependent values. In doing so a renormalized bending rigidity can be expressed as:

$$\frac{\kappa}{k_BT} = \frac{\kappa_0}{k_BT} - \frac{3}{4\pi} \ln \left(\frac{d_{TS}}{2l_c} \right) \quad (2)$$

Here d_{TS} describes the periodicity of the structure and l_c is the effective thickness of the amphiphilic film which in a first approximation is given by the length of a single surfactant molecule. κ_0 denotes the bare bending modulus (rigidity) without the modifications due to thermal fluctuations.

Using the Gauss model of random interfaces *Safran* and *Pieruschka* were able to relate the renormalized membrane rigidity κ to the structural length scales of a bicontinuous microemulsion according to:[6]

[a]*Department of Chemistry, University of Cologne, Luxemburger Str. 116, 50939 Cologne, Germany. E-mail: Thomas.Sottmann@uni-koeln.de; Fax: +49 221 470 5104; Tel: +49 221 470 6308*
[b]*Institut Laue-Langevin, LSS Group, 6 rue Jules Horowitz, 38042 Grenoble, France*
[c]*Jülich Centre for Neutron Science, JCNS, Forschungszentrum Jülich GmbH, Outstation at FRM II, Lichtenbergstr. 1, 85747 Garching, Germany. E-mail: o.holderer@fz-juelich.de; Fax: +49 89 289 10799; Tel: +49 89 289 10707*
[d]*Jülich Centre for Neutron Science JCNS (JCNS-1) & Institute of Complex Systems (ICS), Forschungszentrum Jülich GmbH, 52425 Jülich, Germany*

$$\frac{\kappa}{k_B T} = \frac{10\sqrt{3}\pi}{64}\frac{\xi_{TS}}{d_{TS}} \quad (3)$$

Here ξ_{TS} is the correlation length of the microemulsion. In former studies several parameters influencing the bending rigidity could be identified. It was observed that the renormalization corrected (bare) bending rigidity κ_0 strongly depends on the amphiphilicity of the surfactant.[7] Furthermore, in agreement with eqn (2) it was found that for a given microemulsion system the renormalized bending rigidity κ increases with increasing surfactant concentration due to a suppression of long-range fluctuations of the amphiphilic film. Also several additives were found to have a striking influence on the membrane rigidity. Amphiphilic diblock copolymers were found to stiffen the amphiphilic film,[8–11] whereas homopolymers decrease the bending rigidity.[12,13] However, in all these cases the membrane rigidity could only be influenced by changing the composition of the microemulsion system under investigation.

From a theoretical point of view it would be of great interest to formulate microemulsions whose properties could be changed without changing chemical composition. In this respect microemulsions containing supercritical fluids represent promising model systems, because the density of supercritical fluids, and thus their solvent properties, can strongly be influenced by varying pressure alone. Due to the thermodynamic properties of CO_2, it is a potential candidate for the formulation of supercritical microemulsions. Besides their relevance for fundamental research, supercritical CO_2-miroemulsions have also attracted much attention as potential replacements for common organic solvents in the field of "green" chemistry,[14,15] since CO_2 is cheap, abundant, non-flammable and non-toxic.

Very recently *Schwan et al.* reported the first successful formulation of balanced supercritical CO_2-microemulsions containing equal amounts of water and CO_2 using technical grade Lutensol® surfactants.[16] They found that these systems show the characteristic temperature driven phase inversion from a CO_2-in-water to a water-in-CO_2-microemulsion *via* a balanced CO_2-microemulsion. However, more than 40 wt% surfactant were needed for the formulation of balanced CO_2-microemulsion, a fact that was attributed to a low CO_2-philicity of the hydrocarbon surfactant tail. From extensive investigations of CO_2-rich water-in-CO_2 microemulsions, it turned out that fluorinated or partly fluorinated surfactants are especially suitable for the formulation of efficient $scCO_2$-microemulsion.[15,17–23] Motivated by these results, we found that the solubilization of CO_2 becomes increasingly efficient if the hydrocarbon surfactants are replaced with commercially available perfluoroalkyl-polyglycolether surfactants.[24] Using high pressure SANS experiments the underlying microstructure of these balanced microemulsions was elucidated and a bicontinuous structure with an adjustable characteristic length scale of 180–500 Å was revealed.[25] Furthermore, these SANS measurements yielded the first evidence that the bare bending rigidity κ_0 of the amphiphilic film can be modified by variation of the pressure alone. The absolute values of the bare bending rigidity correspond almost quantitatively to those found for oil containing microemulsions. In these studies we also found that neutron spin-echo (NSE) experiments provide a powerful tool for directly probing the elastic properties of supercritical CO_2-microemulsions.

However, those experiments only gave a first indication of how the properties of supercritical CO_2-microemulsions can be adjusted with pressure. In order to gain a deeper insight into this fascinating field, further systematic studies were conducted on the basis of our results highlighted in ref. 25. Consequently in the present study, we investigate the membrane properties of the bicontinuous microemulsion H_2O/NaCl–$scCO_2$–non-ionic fluorinated surfactant (Zonyl FSO 100 and Zonyl FSN 100) as a function of pressure and composition. Guided by extensive phase behavior measurements, the microstructure of this system was studied as a function of pressure and composition using SANS. Applying the Gaussian model of random interfaces we were able to extract the elastic properties of the amphiphilic film. Additionally pressure dependent NSE measurements have been conducted in order to directly measure the bending rigidity of the membrane.

2 Experimental section

2.1 Materials

The technical grade fluorinated surfactants were commercial polyethyleneglycol–perfluoroalkylether of the type $F–(CF_2)_i–(CH_2CH_2O)_j–H$ (denoted as CF_iE_j) and were supplied by DuPont (Wuppertal, Germany). The surfactants Zonyl FSN 100 (degree of ethoxylation $j \approx 8$ to 12) and Zonyl FSO 100 (degree of ethoxylation $j \approx 6$ to 10) contained 100% active matter. CO_2 (technically pure) was purchased from Linde AG (Munich, Germany). NaCl (quoted >99.5%) was obtained from Fluka (Neu Ulm, Germany). D_2O was purchased from Eurisotop (quoted >99.9%). All components were directly used without further purification. Water (H_2O) was deionized and distilled twice.

2.2 Phase behaviour

Phase behaviour measurements were carried out in an in-house built high pressure viewing cell with variable volume. This cell is equipped with a saplphire ring cylinder ($h = 50$ mm, $\varnothing_{outside} = 40$ mm, $\varnothing_{inside} = 10$ mm) which contained the microemulsion samples. The pressure as well as the volume of the sample can be varied with a screw driven piston, which is inserted into the cell from above. To determine the system pressure, a pressure transducer is inserted in the bottom of the view cell. Thus a determination of the pressure is possible with an accuracy of ±5 bar. To homogenize the samples, a magnetic stirring bar is added to the cell. The respective samples were prepared by weight directly inside the view cell. First a known amount of a NaCl solution (brine, in all cases 1 wt% NaCl in water) was filled in the cell. Then respective amounts of the surfactants were added and dissolved in the NaCl solution at 50 °C. Subsequently the cell was filled with CO_2 using an in-house build filling apparatus equipped with a membrane reservoir. In all cases liquid CO_2 was added at a pressure of $p = 70$ bar and ambient temperature where the density of CO_2 was known. The amount of CO_2 added was determined by volume. Accordingly, the composition of the samples is given by the mass fraction α of CO_2 in the brine/CO_2 mixture and the mass fraction γ of the surfactant in the overall mixture. Mixtures of two surfactants were characterized by δ, the mass fraction of the co-surfactant in the surfactant mixture. For

a given composition the number and type of the occurring phases were determined visually at a constant pressure as a function of temperature using a water bath. The temperature of the water bath was controlled with a precision of ±0.1 °C. The resulting temperature-dependent phase diagram represents vertical $T(\gamma)$ sections through the upright phase prism of the ternary microemulsion system H_2O/NaCl–CO_2–non-ionic surfactant at a constant α (see Fig. 1, right).[26] In such a $T(\gamma)$ section an extended three phase region can be found at intermediate surfactant concentrations and temperatures. With increasing surfactant concentration the three phase region meets the one phase region at the so-called optimum point $\tilde{x}$. At temperatures below and above the one- and three-phase regions, different two phase regions are observed. To determine the phase boundaries of the one phase region the samples were mixed far from the one phase region (deep in the two phase region) and were then slowly transferred into the one phase region by stepwise heating and cooling. Phase boundaries in the three phase region were determined by heating the sample to a defined temperature under stirring. The stirring was then stopped, and after equilibration the number and the type of phases were determined.

2.3 SANS measurements

SANS measurements were carried out on the D11 instrument at the Institut Laue-Langevin (ILL), Grenoble, France.[46] SANS data were recorded at a wavelength of $\lambda = 6$ Å at three detector distances of 1.2, 8 and 34 m. Thus the momentum transfer $q = 4\pi\sin(\theta/2)/\lambda$ ranged from 0.001 to 0.5 Å^{-1}, where θ is the scattering angle. The wavelength distribution was $\Delta\lambda/\lambda = 0.09$ (full width at half maximum). The neutron beam was collimated using a series of 11 movable collimation guides which can be inserted into the beam at a distance of 1.5–40.5 m between the guide and sample. In order to reduce the divergence of the incident beam and thus to increase the resolution, the distance between the guide and sample was chosen to be at least the sample–detector distance.

All SANS measurements were performed using a high pressure (HP) SANS cell with variable volume. In this cell samples are kept between two sapphire windows (thickness 12 mm) and the neutron path length through the sample is 2 mm. The pressure as well as the cell volume can be adjusted automatically with a computer controlled piston which is inserted into the cell from above. The pressure inside the cell is measured with a computerized pressure probe which is inserted in the bottom of the HP-SANS cell. Thus, the pressure can be adjusted with a rather high degree of accuracy (±0.5 bar). In order to control the temperature of the samples, the high pressure SANS cell was connected to a thermostat which allowed a temperature accuracy during the measurement of ±0.05 °C. All samples were directly prepared in the SANS cell. First a known volume of a homogenized brine–surfactant mixture was added to the cell. Then liquid CO_2 was added at 25 °C and 70 bar. The amount of CO_2 was determined by volume. Afterwards, the sample was heated/cooled to the required temperature, adjusted to the desired pressure, and homogenized with the help of a magnetic stirring bar. Visual inspection through the sapphire windows ensured that all samples were homogeneous.

Scattered neutrons were detected by a two-dimensional ^{3}He-gas detector with 128 × 128 detector pixels of 7.5 × 7.5 mm. To prevent overloading by the primary neutron beam, a beam stop was positioned in front of the detector. To obtain a one dimensional scattering spectrum the two dimensional raw data were masked, radially averaged and normalized to the absolute scale using the standard evaluation software available at the ILL. The normalization of the scattering data to the absolute scale was performed using the incoherent scattering of H_2O as reference. All measurements were background corrected. Furthermore, the detector deadtime was corrected during raw data evaluation, finally yielding the differential cross-section $d\sigma(q)/d\Omega$. Datasets from different sample detector distances overlap without scale adjustment. A few data points of the lowest and highest q-values were cut from each measurement.

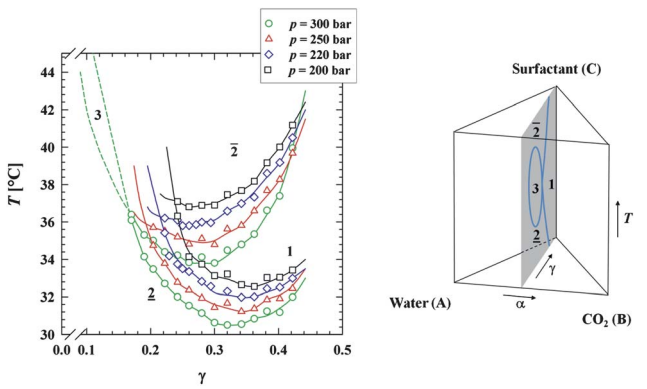

Fig. 1 Left: phase diagram of the microemulsion H_2O/NaCl–CO_2–Zonyl FSO 100/Zonyl FSN 100 at $\alpha = 0.40$ and $\delta = 0.40$. The phase behavior was measured at four different pressures between 200 and 300 bar. With increasing pressure the surfactant solubilizes water and CO_2 more efficiently. Right: schematic drawing of the ternary phase prism.

2.4 NSE measurements

NSE experiments were performed on the J-NSE spectrometer at the Jülich Centre of Neutron Science at the Forschungsreaktor II in Garching, Germany.[27,28] The samples for the NSE measurements were kept in a non-magnetic high pressure NSE cell between two sapphire windows. The neutron path length through the sample is 4 mm. Samples were prepared directly inside the NSE cell. First, a known mass of a homogenized brine–surfactant mixture was added to the cell. Subsequently, the remaining cell volume was filled with CO_2 using a high precision high pressure pump. During the NSE measurements this pump allowed the pressure to be adjusted to ±0.1 bar. The temperature of the NSE samples was controlled to ±0.1 °C using a thermostat. Its water loop was directly connected to the NSE cell. For the homogenization of the samples the high pressure cell (~10 kg) was shaken by hand for about an hour. Before and after each measurement, visual inspection was undertaken to check the homogeneity of the sample.

Interpretation of experimental NSE data from bicontinuous microemulsions in terms of the available theoretical models requires that $q_{max} \ll q$, where q_{max} is the position of the correlation peak. Fortunately, bicontinuous $scCO_2$-microemulsions have a relatively large bulk scattering intensity; still comparatively large scattering angles are accessible, before the incoherent

background level prevents efficient data collection. In this respect, NSE spectra were recorded at five different q values between $q = 0.05$ and $q = 0.18$ Å^{-1} (corresponding to length scales in a real space of $\xi = 2\pi/q = 125$–35 Å). The wavelength used was $\lambda = 8$ Å with a FWHM of $\Delta\lambda/\lambda = 0.1$. The resolution of the NSE spectrometer was determined using graphite powder. For the raw data evaluation the standard software (echodet) available at the JCNS was used.

3 Scattering theory

3.1 Small angle scattering

Small angle neutron scattering experiments allow for the investigation of the structural properties of microemulsions. By adjusting bulk contrast conditions, *i.e.* establishing a scattering contrast between water and oil domains, the periodicity d_{TS} and the correlation length ξ_{TS} can be determined. *Teubner* and *Strey*[29] showed that the bulk scattering curve of balanced microemulsions is quantitatively described by, as well as can be determined from, a description of the scattering curve by the formula:

$$I(q) = \frac{8\pi\phi_a\phi_b\Delta\rho^2/\xi_{TS}}{a_2 + c_1q^2 + c_2q^4} + b, \tag{4}$$

with $\Delta\rho$ being the scattering contrast between brine and CO_2, ϕ_i the volume fractions of the two subphases and b the incoherent scattering background. The free fit parameters a_2, c_1 and c_2 stem from a Landau–Ginzburg order parameter expansion of the local free energy density including gradient terms. $c_1 < 0$ causes a characteristic correlation peak of the scattering curve at nonzero wave vectors. From these parameters the characteristic periodicity d_{TS}, and the correlation length ξ_{TS}, can be deduced.[29,30] The three parameters a_2, c_1 and c_2 may be grouped together within the amphiphilicity factor:

$$f_a = \frac{c_1}{\sqrt{4a_2c_2}} \tag{5}$$

which describes the amphiphilicity of a surfactant. The factor f_a is close to -1 for "good" microemulsions, equal to 0 at the Liftshitz line and equal to +1 at the disordered line, where the characteristic length scale diverges.

Although the *Teubner–Strey* formula is a useful model for the description of the scattering peak of bicontinuous microemulsions, the scattering at high values of q is not quantitatively described. In this regime, which is also denoted as the *Porod* limit, the scattering pattern is adequately described by:

$$\lim_{q\to\infty}\left[I(q)\right] = 2\pi\frac{\Delta\rho^2}{q^4}\frac{S}{V}\exp\left(-q^2t^2\right) + I_{incoh} \tag{6}$$

Here the diffuse nature of amphiphilic film caused by thermal fluctuations and penetration of solvent molecules into the membrane is taken into account by convoluting the usual step profile of a sharp interface with a smooth *Gaussian* profile of width t.[31] Eqn (6) allows extraction of the specific internal interface $S/V = \phi_{C,i}/l_c$ given by the volume fraction of the surfactant in the internal interface $\phi_{C,i}$ and the effective thickness of the amphiphilic film l_c. Details are found in the literature.[32]

3.2 Inelastic scattering

At large wave vectors $q_{max} \ll q$ thermally induced local undulations of the amphiphilic film are probed. Describing the amphiphilic film by a randomly oriented assembly of finite membrane patches *Zilman* and *Granek* proposed an approximative expression of the dynamic structure factor for bicontinuous microemulsions valid at large q,[33]

$$S(q,t) = S(q)\exp\left(-(\Gamma_q t)^\beta\right) \tag{7}$$

with $\beta = 2/3$ and the q-dependent relaxation

$$\Gamma_q = 0.025\gamma_k\left(\frac{k_BT}{\kappa_0}\right)^{1/2}\frac{k_BT}{\eta}q^3 \tag{8}$$

Here η is the average viscosity of the solvents on both sides of the surfactant membrane and $\gamma_k \cong 1 - 3(k_BT/4\pi\kappa_0)\ln(q\xi_{TS})$. This model has been applied successfully to interpret NSE experiments on microemulsions.[34,35]

Thus the *Zilman–Granek* model directly relates the bending rigidity of the surfactant membrane to its relaxation rate. A quantitative determination of the bending rigidity with the *Zilman–Granek* theory, however, requires that not all the approximations leading to eqn (8) are carried out, but numerical integrations of the expression of a fluctuating membrane patch are used instead.[11] In this case the dynamic structure factor can be rewritten as:

$$S(q,t) \propto \int_0^1 d\mu \int_0^{r_{max}} dr r J_0\left(qr\sqrt{1-\mu^2}\right)$$

$$\times \exp\left[-k_BT/(2\pi\kappa_0)q^2\mu^2\int_{k_{min}}^{k_{max}} dk\frac{1 - J_0(kr)e^{-\omega(k)t}}{k^3}\right] \tag{9}$$

where the real space upper cutoff is set to $r_{max} \approx \pi/k_{min} = \xi_{TS}/\varepsilon$ with k being the undulation wave vector. The parameter ε is expected to be $\varepsilon \approx 1$. It takes into account any deviations due to the assumption of a sharp cut-off of the considered membrane patch. The integration over μ, the cosine of the angle between q and the membrane surface normal, affects the angular averaging over patch orientations. In eqn (9) $\omega(k)$ is the most simple dispersion relation of the undulation modes of a free planar membrane in a viscous liquid $\omega(k) = (\kappa_0/4\eta)k^3$. The upper cut of the mode wave vector, $k_{max} = \pi/l_c$, accounts for the finite size of the surfactant molecules, but has only a marginal influence on the result. The only free fitting parameter in eqn (9) is the bending rigidity κ_0 in the dispersion relation. By integrating over the undulation mode wave vectors k all contributions from undulation modes are explicitly taken into account, and thus κ_0 represents the bare bending rigidity of the membrane.

4 Results and discussion

First the phase behavior of the balanced CO_2-microemulsion H_2O/NaCl–CO_2–Zonyl FSO 100/Zonyl FSN 100 is shown in detail (Section 4.1). Subsequently, the results obtained from small angle neutron scattering experiments are presented in Section 4.2. Here, both the microstructure and the elastic properties obtained from SANS measurements are discussed. In

Section 4.3 the NSE results are shown and compared to those obtained from SANS.

4.1 Phase behaviour

A convenient way to characterize the phase behavior of balanced microemulsions is to perform a cut through the ternary phase prism water–oil (or in this case CO_2)—surfactant at a constant mass fraction α of CO_2 in the brine/CO_2 mixture. The sequence of occurring phases is then determined as a function of the temperature and the overall surfactant mass fraction γ. In Fig. 1 (left) the experimental phase diagram of the system H_2O/NaCl–CO_2–Zonyl FSO 100/Zonyl FSN 100 is shown at four different pressures in a range from $p = 200$–300 bar. The phase behavior was determined at a constant α of 0.40 and $\delta = 0.40$ (mass fraction of Zonyl FSN 100 in the surfactant mixture). 1 wt% NaCl was added to the aqueous phase in order to screen ionic interactions caused by impurities.

For all pressures a phase sequence can be observed which is typical for balanced microemulsions formulated with nonionic surfactants.[2] At low temperatures a two phase coexistence ($\underline{2}$) of a CO_2-in-water (c/w)-microemulsion with a CO_2 excess phase is found, while at high temperatures a coexistence of a water-in-CO_2 microemulsion with a water-excess phase ($\bar{2}$) occurs. This phase inversion is triggered by a decrease of the spontaneous curvature c_0 of the amphiphilic film caused by an increase of the temperature.[36] It manifests itself by an extended three phase region (3) that can be observed at intermediate temperatures and surfactant weight fractions γ. With increasing surfactant concentration the three phase region meets the one phase region at the so-called optimum point $\tilde{X}$ (at $\tilde{\gamma}$ and $\tilde{T}$). It defines the minimum amount of surfactant needed to solubilize water and CO_2 at the phase inversion temperature. Thus, the $\tilde{X}$-point indicates the efficiency of the surfactant to emulsify given amounts of water and CO_2.

The results shown in Fig. 1 clearly indicate that the phase behavior of the system H_2O/NaCl–CO_2–Zonyl FSO 100/Zonyl FSN 100 is strongly influenced by the pressure. Fig. 2 illustrates the dependence of the optimum point $\tilde{X}$, *i.e.* $\tilde{\gamma}$ and $\tilde{T}$, on pressure. Note that for the sake of clarity the phase diagrams for pressures lower than 200 bar are not shown in Fig. 1. With increasing pressure the surfactant weight fraction $\tilde{\gamma}$ at the optimum point decreases considerably, *i.e.* the ability of the surfactant to solubilize water and $scCO_2$ strongly increases. Simultaneously the phase inversion temperature $\tilde{T}$ is slightly shifted to lower temperatures. Both findings can be explained by the improved CO_2 solvent properties which exist at high pressures. They lead to an enhanced CO_2–surfactant interaction and thus to a better solvatization of the hydrophobic surfactant tails by CO_2 molecules which allows for a more efficient microemulsion formulation. Furthermore the increasing solvatization of the surfactant tails by CO_2 molecules also increases the curvature of the surfactant membrane around the water which causes the shift of $\tilde{T}$ to lower temperatures.

4.2 Microstructure

The microstructure of the system H_2O/NaCl–$scCO_2$–Zonyl FSO 100/Zonyl FSN 100 at $\varepsilon = 0.01$, $\alpha = 0.40$ and $\delta = 0.40$ was investigated as a function of pressure and composition. All SANS measurements were performed at a temperature in the middle of the one phase region (see Table 1). In order to improve the scattering contrast H_2O was replaced with D_2O whereby the molar fraction of water molecules was kept constant. Note that due to the higher molar mass of D_2O the weight fraction α of CO_2 in the D_2O–CO_2 mixture as well as the overall surfactant weight fraction in the microemulsion decrease slightly. However in order to avoid confusion in the following discussion, all composition variables are related to the respective H_2O samples. Please also note that the phase boundaries are shifted to lower temperatures ($\Delta T \approx 2$ to 3 K) if H_2O is replaced with D_2O.

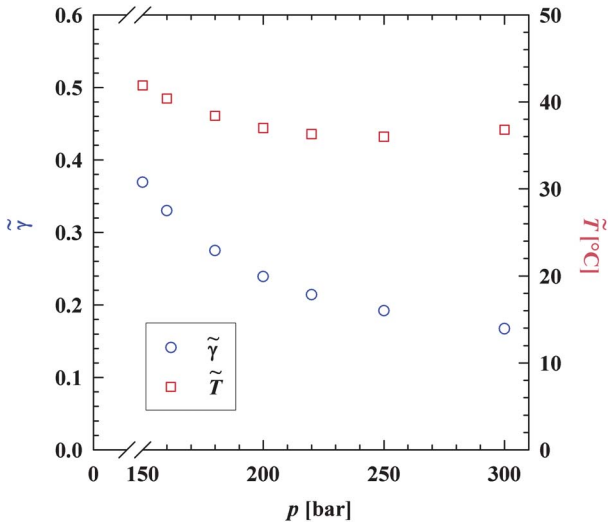

Fig. 2 Variation of $\tilde{\gamma}$ and $\tilde{T}$ as a function of pressure p for balanced microemulsion systems of the type H_2O/NaCl–CO_2–Zonyl FSO 100/Zonyl FSN 100 at $\alpha = 0.40$ and $\delta = 0.40$. With increasing pressure the microemulsion becomes increasingly efficient whereas simultaneously the phase inversion temperature is shifted to lower temperatures. Both findings can be explained with improved CO_2-solvent properties at high pressures.

(i) Influence of concentration. In a first set of experiments the microstructure of the $scCO_2$-microemulsion was studied at a constant pressure of $p = 220$ bar. The SANS data recorded at $\gamma = 0.244$, 0.262 and 0.350 are shown in Fig. 3. For all three compositions a pronounced scattering peak is observed at intermediate q values. The shape of these scattering curves in combination with the information obtained from phase behavior measurements strongly supports the existence of a bicontinuous microemulsion structure.[37,38] The position of the correlation peak is directly related to the periodicity d_{TS} of the bicontinuous structure by $q_{max} \approx 1/d_{TS}$. The shift of the correlation peak to lower q values, which can be observed as the surfactant mass fraction increases, indicates a decrease of the periodicity of the microstructure. Furthermore, with decreasing surfactant weight fraction the correlation peak becomes less pronounced indicating a loss of the structural order. At large q values the correlation peak is followed by a steep $\exp(-q^2t^2)q^{-4}$ decay of the scattering intensity. Small deviations from an ideal q^{-4} decay at very high q values already indicate that the scattering length density profile of the water–CO_2 interface is not sharp and can thus not be modeled by a step profile.

Table 1 Structural parameters obtained from the analysis of the scattering data of the microemulsion system H_2O/NaCl–CO_2–Zonyl FSO 100/Zonyl FSN 100 at $\alpha = 0.40$ and $\delta = 0.40$. From the analysis of the peak region the characteristic periodicity d_{TS}, the correlation length ξ_{TS} and the amphiphilicity factor f_a were obtained. Analysis of the high q region yields the specific internal interface S/V and the volume fraction of the surfactant in the internal interface $\phi_{c,i}$

γ	T/°C	ϕ_c	p/bar	d_{TS}/Å	ξ_{TS}/Å	$-f_a$	S/V/Å^{-1}	t/Å	$\phi_{c,i}$
0.244	32.9	0.186	220	332.8	121.8	−0.682	0.0171	5.30	0.146
0.262	33.0	0.270	200	279.1	114.5	−0.738	0.0141	5.95	0.248
0.262	32.3	0.274	220	287.4	120.6	−0.784	0.0140	5.75	0.251
0.262	31.7	0.275	250	289.8	130.6	−0.807	0.0137	5.50	0.252
0.262	31.1	0.277	300	291.9	134.6	−0.787	0.0135	5.40	0.255
0.350	34.9	0.280	160	188.4	106.6	−0.853	0.0202	6.70	0.263
0.350	32.4	0.199	200	185.8	106.9	−0.858	0.0206	6.75	0.171
0.350	31.7	0.200	220	184.4	104.3	−0.853	0.0208	6.90	0.168
0.350	30.7	0.202	250	182.5	101.7	−0.849	0.0210	7.30	0.167
0.350	29.9	0.204	300	176.3	93.3	−0.834	0.0216	7.30	0.164

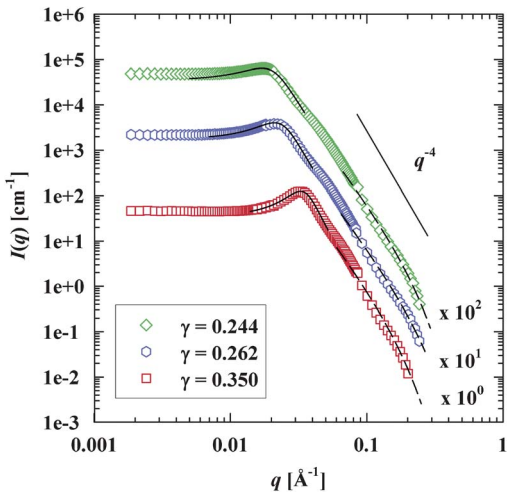

Fig. 3 Bulk scattering curves of balanced CO_2-microemulsions of the system D_2O/NaCl–CO_2–Zonyl FSO 100/Zonyl FSN 100 at $\alpha = 0.40$, $\delta = 0.40$, $p = 220$ bar and three different surfactant weight fractions. The *Teubner–Strey* model and the *Porod* model have been used in order to describe the peak region (solid lines) and the high q-range part (dashed lines), respectively. Note that to aid viewing the scattering curves are multiplied with appropriate factors.

In order to analyze the correlation peak, the *Teubner–Strey*[29] model was applied (solid lines). Additionally, the *Porod* model for diffuse interfaces was used to describe the high q regime of the scattering spectra (dashed line).[31] As is evident, both models describe the respective parts of the experimental scattering data nearly quantitatively. The parameters obtained by the analysis of the scattering data are listed in Table 1.

These results confirm the trends that were obtained from a qualitative interpretation of the scattering curves. The periodicity d_{TS} of the microstructure was found to steadily decrease with increasing surfactant weight fraction from $d_{TS} = 331$ Å at $\gamma = 0.144$ to $d_{TS} = 184$ Å at $\gamma = 0.350$. This observation arises from the fact that the total interfacial area of the amphiphilic film grows as the surfactant mass fraction increases, which hence leads to the formation of smaller microemulsion domains. Consequently, the specific internal interface S/V increases from $S/V = 0.0105$ Å^{-1} at $\gamma = 0.244$ to $S/V = 0.0182$ Å^{-1} at $\gamma = 0.350$.

From the specific internal interface S/V the volume fraction of the surfactant in the amphiphilic film $\phi_{c,i}$ can be calculated using $\phi_{c,i} = l_c S/V$. Here, the length l_c of a single surfactant molecule was estimated to be 14 Å. The values obtained for $\phi_{c,i}$ are also listed in Table 1. Since $\phi_c > \phi_{c,i}$ a significant fraction of the surfactant is dissolved in the $scCO_2$ domains.

As described above, the correlation peak of the scattering spectra becomes less pronounced if the surfactant weight fraction is decreased which indicates a loss of structural order.[7] This finding correlates with the dependence of the amphiphilicity factor f_a on the surfactant weight fraction, which is found to increase from $f_a = -0.853$ to $f_a = -0.682$ as the surfactant weight fraction was decreased from $\gamma = 0.350$ to 0.244.

In order to understand this loss of structural order we used the Gaussian model of random interfaces (eqn (3)) and the structural parameters d_{TS} and ξ_{TS} to calculate the renormalized bending rigidity κ_{SANS}. Note that the index SANS is added to distinguish between the bending rigidity obtained from SANS and NSE. In Fig. 4 κ_{SANS} is shown as a function of the surfactant weight fraction γ. As can be seen, with increasing γ the renormalized bending rigidity κ_{SANS} increases by almost 50% from $\kappa_{SANS} = 0.31\ k_BT$ at $\gamma = 0.244$ to $\kappa_{SANS} = 0.48\ k_BT$ at $\gamma = 0.350$. Hence, an increase of the surfactant weight fraction leads to a stiffening of the surfactant membrane. This stiffening of the amphiphilic film is caused by the suppression of thermally induced membrane fluctuations at high surfactant weight fraction and small structural length scales, respectively. The absolute values of κ_{SANS} in the bicontinuous $scCO_2$-microemulsions studied here are of similar magnitude as the values obtained for surfactant membranes in H_2O–n-alkane–C_iE_j microemulsions.[7]

Since the renormalized bending rigidity κ_{SANS} lumps together all effects from membrane fluctuations up to a wavelength corresponding to the structural dimension, it differs from the "bare" bending rigidity $\kappa_{0,SANS}$ of the membrane by a renormalization factor, which depends for a given system on the characteristic length scale $\xi = d_{TS}/2$ of the microemulsion[39–42] (eqn (2)). For a given microemulsion system the renormalization corrected bending rigidity of the amphiphilic film, $\kappa_{0,SANS}$, should be constant irrespective of the surfactant weight fraction. The $\kappa_{0,SANS}$ values obtained using eqn (2) are also shown in Fig. 4. As expected $\kappa_{0,SANS}$ was found to be almost constant, *i.e.* $\kappa_{0,SANS} \approx 0.91 \pm 0.01\ k_BT$.† Again, this value corresponds

† The given error is the statistical variation of the fit parameter κ.

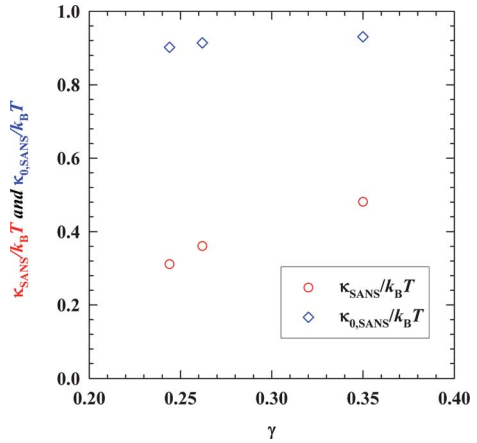

Fig. 4 Bending rigidity κ_{SANS} and the renormalization corrected bending rigidity $\kappa_{0,SANS}$ for CO_2-microemulsions of the type D_2O/NaCl–CO_2–Zonyl FSO 100/Zonyl FSN 100 at $\varepsilon = 0.01$, $\alpha = 0.40$, $\delta = 0.40$ and $p = 220$ bar plotted as a function of the surfactant mass fraction γ. With increasing surfactant concentration κ_{SANS} increases due to a suppression of thermally induced long-range fluctuations of the amphiphilic film. The renormalization corrected bending rigidity $\kappa_{0,SANS}$ is nearly independent of the surfactant mass fraction.

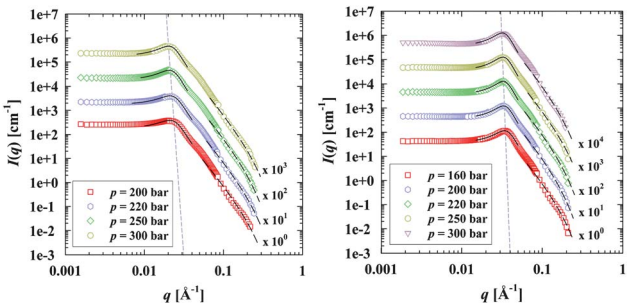

Fig. 5 Bulk scattering curves of balanced CO_2-microemuslions of the type D_2O/NaCl–CO_2–Zonyl FSO 100/Zonyl FSN 100 at $\varepsilon = 0.01$, $\alpha = 0.40$ and $\delta = 0.40$. The SANS spectra were recorded at $\gamma = 0.266$ (left) and $\gamma = 0.350$ (right), respectively. At $\gamma = 0.262$ the pressure was varied from 200 to 300 bar whereas at $\gamma = 0.350$ a pressure range from 160–300 bar was covered. The scattering data were analyzed using the *Teubner–Strey* model (solid lines) and the *Porod* model for diffuse interfaces (dashed lines) was used.

almost quantitatively to the renormalization corrected bending rigidity of oil containing microemulsions which is of the order of 1 k_BT.

(ii) Influence of pressure. So far the influence of the surfactant mass fraction on the microstructure of the $scCO_2$-microemulsion H_2O/NaCl–CO_2–Zonyl FSO 100/Zonyl FSN 100 at $\varepsilon = 0.01$, $\alpha = 0.40$ and $\delta = 0.40$ was studied at a constant pressure of $p = 220$ bar. In the next step the pressure dependence of the microstructure was studied at two surfactant weight fractions of $\gamma = 0.266$ and $\gamma = 0.350$. At these two γ-values the width of the one phase region allows the examination of the pressure dependence between $p = 200$ and 300 bar at $\gamma = 0.266$ and between $p = 160$ and 300 bar at $\gamma = 0.350$, respectively. In Fig. 5 the obtained bulk-contrast scattering curves are shown.

As is evident, all scattering curves exhibit a correlation peak which is typical for bicontinuous microemulsions followed by the exp $(-q^2t^2)q^{-4}$ decay of the scattering intensity at large q values. For both surfactant weight fractions a shift of the correlation peak to slightly lower q values occurs with increasing pressure indicating a slight increase of the periodicity of the microstructure. Simultaneously the correlation peak becomes more pronounced which indicates a higher structural order of the microemulsion at high pressure. The scattering data were again analyzed using the *Teubner–Strey* formula (solid lines) and the *Porod* model for diffuse interfaces (dashed lines). In Table 2 the characteristic periodicity d_{TS}, the correlation length ξ_{TS} and the amphiphilicity factor f_a obtained are compiled.

Again, these results confirm the trends that were obtained from a qualitative interpretation of the experimental scattering data. Thus, for both surfactant concentrations a slight increase of the periodicity d_{TS} can be observed with increasing pressure. At first glance this pressure dependence of d_{TS} seems to be somewhat counterintuitive since an increase of the pressure leads to a compression of the $scCO_2$ domains and hence one would expect a decrease of the periodicity. However, from the analysis of the high q-regime of the scattering spectra it was found that with increasing pressure the specific internal interface S/V is reduced (see Table 3). This in turn requires the formation of larger microemulsion domains. In conjunction with S/V the volume fraction of the surfactant in the amphiphilic film $\phi_{c,i}$ also decreases slightly with increasing pressure as a result of an enhanced monomeric solubility of surfactant in $scCO_2$.

The pressure dependence of the amphiphilicity factor f_a indicates that with increasing pressure a microemulsion with higher structural order is formed. In order to understand this influence of the pressure on both the microstructure and the phase behavior of balanced $scCO_2$ microemulsions (Fig. 1), the bending elastic constants κ_{SANS} and $\kappa_{0,SANS}$ were calculated from the structural parameters using eqn (2) and (3) respectively. The values obtained are plotted in Fig. 6 as a function of the pressure.

The results presented in Fig. 6 clearly show that for both surfactant weight fractions both the renormalized bending rigidity κ_{SANS} and the renormalization corrected ("bare") rigidity $\kappa_{0,SANS}$ increase with increasing pressure. At $\gamma = 0.262$ κ_{SANS} increases by almost 12% from $\kappa_{SANS} = 0.35\ k_BT$ at $p = 200$ bar to $\kappa_{SANS} = 0.39\ k_BT$ at $p = 300$ bar. At $\gamma = 0.350$ a somewhat weaker pressure dependence of κ_{SANS} is observed. Here, the renormalized bending rigidity increases from $\kappa_{SANS} = 0.45\ k_BT$ at $p = 160$ bar to $\kappa_{SANS} = 0.48\ k_BT$ at $p = 300$ bar. Note that the

Table 2 Structural parameters obtained from the analysis of the scattering peak of the system D_2O/NaCl–CO_2–Zonyl FSO 100/Zonyl FSN 100 at $\varepsilon = 0.01$, $\alpha = 0.40$, $\delta = 0.40$ at various pressures and compositions

γ	p/bar	T_{SANS}/°C	d_{TS}/Å	ξ_{TS}/Å	$-f_a$
0.262	200	33.0	277.1	114.5	−0.739
	220	32.3	284.2	120.6	−0.754
	250	31.7	287.4	130.6	−0.785
	300	31.1	292.0	134.6	−0.787
0.350	160	34.9	176.3	93.3	−0.834
	200	32.4	182.5	101.7	−0.849
	220	31.7	184.4	104.4	−0.853
	250	30.7	185.8	106.9	−0.858
	300	29.9	188.4	106.6	−0.853

Table 3 Structural parameters obtained from the analysis of the large q-regime of the scattering data of the microemulsion system D_2O/NaCl–CO_2–Zonyl FSO 100/Zonyl FSN 100 at $\alpha = 0.40$, $\delta = 0.40$ at various pressures and compositions

γ	p/bar	T_{SANS}/°C	ϕ_c	S/V/Å^{-1}	t/Å	$\phi_{c,i}$
0.262	200	33.0	0.199	0.0123	4.7	0.172
	220	32.3	0.200	0.0121	4.9	0.169
	250	31.7	0.202	0.0119	5.0	0.167
	300	31.1	0.204	0.0118	4.7	0.165
0.350	160	34.9	0.263	0.0188	5.5	0.263
	200	32.4	0.274	0.0184	5.8	0.258
	220	31.7	0.275	0.0182	5.9	0.254
	250	30.7	0.278	0.0181	5.5	0.253
	300	29.9	0.280	0.0179	5.9	0.251

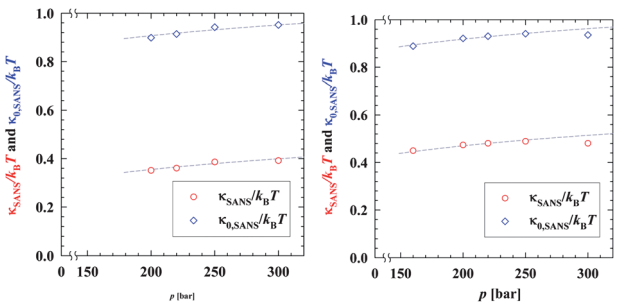

Fig. 6 Pressure dependence of the renormalized bending rigidity κ_{SANS} and the bare bending rigidity $\kappa_{0,SANS}$ of the amphiphilic film in the $scCO_2$-microemulsion D_2O/NaCl–CO_2–Zonyl FSO 100/Zonyl FSN 100 ($\alpha = 0.40$, $\delta = 0.40$). The bending elastic constants were determined from pressure dependent SANS-measurements which were performed at $\gamma = 0.262$ (left) and $\gamma = 0.350$ (right).

higher κ_{SANS} values found at $\gamma = 0.350$ are a result of the suppression of thermally induced membrane fluctuations at high surfactant mass fraction, *i.e.* small structural length scales. The renormalization corrected bending rigidity $\kappa_{0,SANS}$ which was found to be nearly independent of the surfactant weight fraction (see also Fig. 4) increases for both compositions from $\kappa_{0,SANS} = 0.90$ to 0.95 k_BT in the pressure range from 200–300 bar.

These results strikingly demonstrate that the bending elastic properties of the supercritical CO_2-micreomulsions can be influenced simply by a variation of the pressure at a fixed microemulsion composition. This stiffening of the membrane at high pressures manifests itself in the higher order of the microemulsion structure as well as in an increased ability of the surfactant to solubilize water and $scCO_2$. A possible explanation for this finding might be improved interactions between $scCO_2$ and the surfactant tails at high pressures. In contrast to oil containing microemulsions the additional tuning parameter of "pressure" allows the properties of $scCO_2$-microemulsions to be tuned at fixed composition.

4.3 Dynamics

While the bare bending rigidity κ_0 can only be extracted indirectly from the analysis of the SANS curves, a direct determination of the elastic properties of surfactant membranes is possible upon studying the dynamic properties of bicontinuous $scCO_2$-microemulsions with the help of quasielastic scattering. Among these techniques neutron spin-echo (NSE) spectroscopy is the one with the highest energy resolution and—due to the covered q-range—provides a means to study the dynamics of mesoscopic objects. Furthermore, the decay time τ_d for thermally activated fluctuations of surfactant membrane patches is in the regime of nanoseconds and therefore well inside the time window of NSE spectroscopy.

Bulk contrast NSE-measurements were performed on the bicontinuous $scCO_2$-microemulsion D_2O/NaCl–CO_2–Zonyl FSO 100/Zonyl FSN 100 at $\varepsilon = 0.01$, $\alpha = 0.40$, $\delta = 0.40$ and $\gamma = 0.262$. The microstructure of the same system was studied in the previous section with pressure dependent SANS investigations. The NSE experiments were performed under the same experimental conditions. Again a pressure range from $p = 200$ to 300 bar was explored, while the sample temperature was adjusted to the middle of the one phase region. Fig. 7 (right) shows the normalized intermediate scattering function $S(q,\tau)$ recorded at a pressure of $p = 300$ bar for five different q values. For a first evaluation of the experimental data, the analytical solution of the *Zilman–Granek* model was applied (eqn (7)). For the viscosity, the average of the viscosities of water and $scCO_2$ was used. Fitting the experimental $S(q,t)$ data for each of the q values separately with the expression of eqn (7) shows that the q^3 dependence of the relaxation rate Γ_{ZG}, which is predicted for bicontinuous microemulsions according to eqn (8), is found also for bicontinuously structured supercritical CO_2-microemulsion. In addition, the typical stretching exponent of $\beta_{ZG} = 2/3$ was obtained (see Fig. 7, left). However, compared to microemulsions consisting of *n*-decane, water and $C_{10}E_4$ which form bicontinuous structures at similar surfactant mass fractions, the relaxation rate is faster by roughly a factor of two.[11] The average viscosity which is about half the value in the supercritical microemulsion compared to oil–water microemulsions partly accounts for this effect.

Upon calculation of the bending rigidity from eqn (7), a value which was considerably larger than the expected one (of the order of k_BT) was obtained. Thus, in order to enable

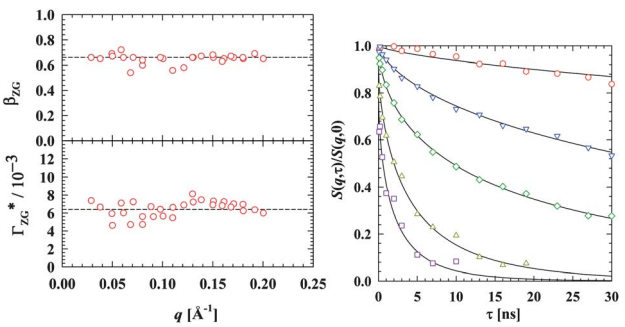

Fig. 7 Left: stretching exponent β_{ZG} and reduced relaxation rate $\Gamma_{ZG}^* = (\Gamma_{ZG}/q^3)(\eta_0/k_BT/\gamma_k)$ obtained from the *Zilman–Granek* analysis of the NSE data of the $scCO_2$-microemulsion D_2O/NaCl–$scCO_2$–Zonyl FSO 100/Zonyl FSN 100 at $\varepsilon = 0.01$, $\alpha = 0.40$, $\delta = 0.40$, $\gamma = 0.262$ and a pressure of $p = 300$ bar. The dashed lines represent $\beta_{ZG} = 2/3$ and the average value of Γ_{ZG}^*. Right: intermediate scattering function $S(q,\tau)$ of the sample reflecting the membrane dynamics on local length scales. The experimental data are fitted with the Zilman–Granek model (eqn (7)). The q values adjusted were 0.05, 0.08, 0.11, 0.15, and 0.18 Å^{-1}.

a quantitative determination of the bending rigidity $\kappa_{0,NSE}$ with the *Zilman–Granek* theory, a numerical integration of the expression of a fluctuating membrane patch must be used instead (eqn (9)).[11,43] Systematic NSE investigations of oil containing microemulsions revealed that the real space upper cut-off $r_{max} \approx \pi/k_{min} = \xi_{TS}/\varepsilon_{ZG}$ of this integration has a significant influence on the resulting values of $\kappa_{0,NSE}$. For this reason, in former studies on oil containing microemulsions the parameter ε_{ZG} was calibrated by fitting the experimental NSE data of an arbitrarily chosen system such that the condition $\kappa_{0,NSE} = \kappa_{0,SANS}$ with $\kappa_{0,SANS}$ being the bare bending rigidity obtained from SANS, is fulfilled. It was found that for $1 \leq \varepsilon_{ZG} \leq 1.3$ the resulting values of $\kappa_{0,NSE}$ are consistent with SANS results. In this work we used a value of $\varepsilon_{ZG} = 1.126$, which was determined from oil containing microemulsions,[43] since not enough reliable data are available in order to calibrate ε for $scCO_2$-microemulsions.

In Fig. 8 the bending rigidity $\kappa_{0,NSE}$ obtained from the analysis of the NSE experiments at $p = 300$, 250 and 200 bar using the integral version of the *Zilman–Granek* model of fluctuating membrane patches is shown as a function of scattering vector q. For comparison the renormalization corrected bending rigidity $\kappa_{0,SANS}$ determined from SANS is also shown (dashed lines). $\kappa_{0,NSE}$ slightly increases with increasing q, until it reaches a plateau at high q values.

The pressure dependence of the bending rigidity $\kappa_{0,NSE}$ confirms the qualitative results obtained from SANS measurements. In our NSE experiments, a significant increase of $\kappa_{0,NSE}$ with increasing pressure was observed. Comparing the absolute values of $\kappa_{0,SANS}$ and $\kappa_{0,NSE}$, however, it turns out that the bending rigidities determined by the means of NSE are somewhat smaller than the bare bending rigidities determined from SANS. In addition, $\kappa_{0,NSE}$ shows a slightly stronger pressure dependence.

These small deviations between $\kappa_{0,NSE}$ and $\kappa_{0,SANS}$ might be caused by uncertainties in the renormalization factor $3/4\pi \ln(d_{TS}/2l_c)$ used for the calculation of $\kappa_{0,SANS}$. Here, the effective thickness of the amphiphilic film l_c could only be estimated although it is an important parameter which has a significant influence on the absolute value of $\kappa_{0,SANS}$. In addition, the $\kappa_{0,NSE}$ values might also be affected by uncertainties due to the still simplifying theoretical model and approximations therein. Furthermore, by using the average viscosity of only the solvents, the energy dissipation in the surfactant layer due to its viscosity is not taken into account. Previous studies on bilayer membranes showed that the energy dissipation in the membrane is not negligible.[44,45] Note that eqn (3) may contain contributions from the saddle splay modulus. Their possible influence on the deviations between $\kappa_{0,NSE}$ and $\kappa_{0,SANS}$ will be scrutinized in our coming investigations.

Nevertheless, despite these minor deviations, there is a good overall agreement between the results obtained from the different experimental techniques. This finding is supported by an additional series of pressure dependent NSE measurements on the system D_2O/NaCl–CO_2–Zonyl FSO 100/Zonyl FSN 100 at $\varepsilon = 0.01$, $\alpha = 0.40$ and $\delta = 0.40$, which were performed at a surfactant weight fraction of $\gamma = 0.35$ in a pressure range between 160 and 300 bar. In these experiments, the pressure dependence of the bending rigidity $\kappa_{0,NSE}$ also confirms the qualitative results obtained from SANS measurements (Fig. 9). The slight deviation

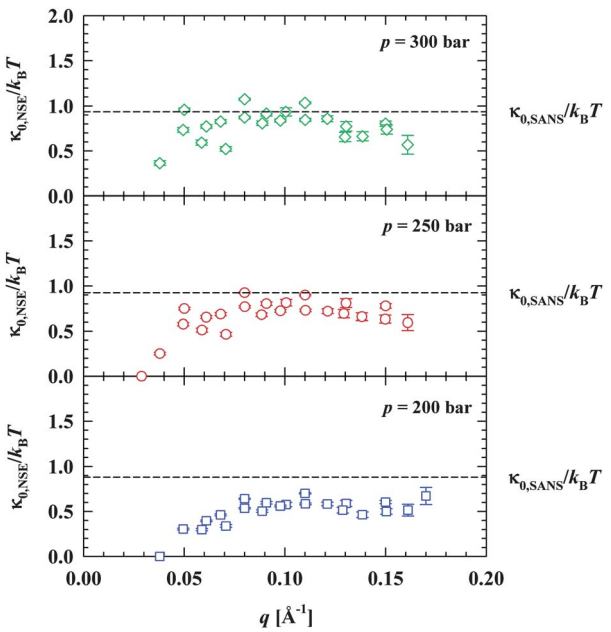

Fig. 8 Bending rigidity $\kappa_{0,NSE}$ of the surfactant membrane in the $scCO_2$-microemulsion D_2O/NaCl–CO_2–Zonyl FSO 100/Zonyl FSN 100 at $\varepsilon = 0.01$, $\alpha = 0.40$, $\delta = 0.40$, $\gamma = 0.262$ and three different pressures between 200 and 300 bar. The $\kappa_{0,NSE}$ values were determined using the numerical solution of the *Zilman–Granek* model. For comparison the renormalization correct bending rigidity $\kappa_{0,SANS}$ is shown (dashed lines).

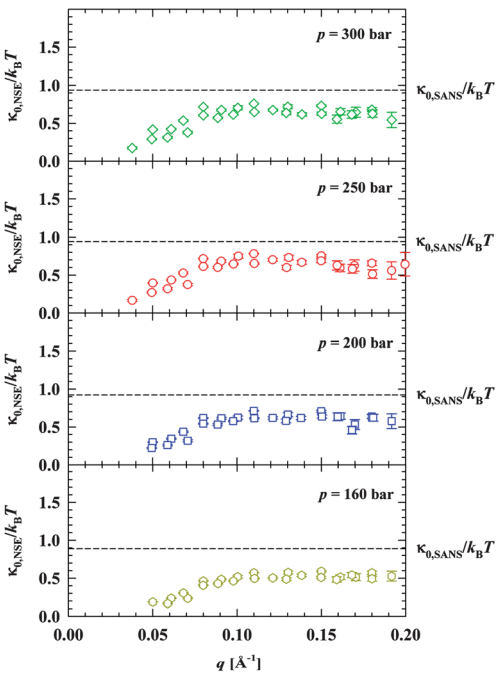

Fig. 9 Bending rigidity $\kappa_{0,NSE}$ of the surfactant membrane in the supercritical CO_2-microemulsion D_2O/NaCl–CO_2–Zonyl FSO 100/Zonyl FSN 100 at $\varepsilon = 0.01$, $\alpha = 0.40$, $\delta = 0.40$ and $\gamma = 0.350$ and four different pressures between 160 and 300 bar. The $\kappa_{0,NSE}$ values were determined with the numerical solution of the *Zilman–Granek*. For comparison the renormalization correct bending rigidity $\kappa_{0,SANS}$ is shown (dashed line).

between the NSE results and the renormalization corrected bending rigidity $\kappa_{0,SANS}$ determined from SANS can be ascribed to the arguments given above.

5 Conclusions

In order to gain a deeper understanding of the properties of supercritical CO_2-microemulsions, we systematically investigated the phase behavior, the microstructure, and the dynamics of balanced $scCO_2$-microemulsions containing equal volumes of water and CO_2. The system under investigation, H_2O/NaCl–CO_2–Zonyl FSO 100/Zonyl FSN 100, shows a temperature dependent phase behavior which follows the general patterns found for nonionic microemulsions. Upon studying the influence of the pressure systematically, we found that the ability of the nonionic fluorosurfactants to solubilize water and CO_2 strongly increases with increasing pressure.

The microstructure of balanced $scCO_2$-microemulsions was investigated as a function of surfactant concentration and pressure using small angle neutron scattering. The scattering data together with results of the phase behavior studies strongly support the existence of bicontinuous structures. From a quantitative analysis of the scattering data using the *Teubner–Strey* approach, we found that at constant pressure the characteristic periodicity d_{TS} of the microemulsion decreases with increasing surfactant weight fraction γ from 332 Å to 184 Å.

The analysis of the SANS data according to the random field model yielded the renormalized bending rigidity κ_{SANS} as well as the renormalization corrected rigidity $\kappa_{0,SANS}$, both of which correspond almost quantitatively to the values obtained for oil containing microemulsions. Thus, κ_{SANS} was found to increase with increasing surfactant weight fraction as a result of suppressed thermally induced membrane fluctuations at large surfactant concentrations and small length scales. $\kappa_{0,SANS}$ on the other hand was found to be independent of γ, *i.e.* $\kappa_{0,SANS} \approx 0.92\ k_BT$.

SANS measurements that were performed at a constant surfactant weight fraction as a function of pressure revealed an increase of the microemulsion domain size with increasing pressure. This somewhat counterintuitive trend was attributed to an enhanced monomeric solubility of the surfactant in $scCO_2$ at high pressures, which leads to a decrease of the membrane volume fraction $\phi_{c,i}$. Upon calculating the bending elastic constant κ_{SANS} and $\kappa_{0,SANS}$ from the structural parameters, we surprisingly found that by increasing the pressure from 200 to 300 bar, the renormalization corrected (bare) bending rigidity $\kappa_{0,SANS}$ and thus the stiffness of the amphiphilic film increase from 0.90 to 0.95 k_BT.

Since SANS measurements only allow an indirect determination of elastic properties of the amphiphilic film, high-pressure neutron spin echo (NSE) measurements were conducted in order to investigate the dynamics of $scCO_2$-microemulsions. We found that fluctuations of the surfactant membranes are directly probed at q values that correspond to a length scale smaller than the average membrane–membrane distance. The numerical form of the *Zilman–Granek* model was found to be the method of choice for the quantitative analysis of the dynamic structure factor. Upon comparing the values of the bare bending rigidity determined by the means of NSE ($\kappa_{0,NSE}$) with those determined by SANS ($\kappa_{0,SANS}$) we found that $\kappa_{0,NSE}$ is only somewhat smaller than $\kappa_{0,SANS}$. The remaining difference might be an indication that contributions of the saddle splay modulus to the bending rigidity κ_{SANS}, which are not covered by the Gaussian random field theory (eqn (3)), play a role. Furthermore the NSE results, a more direct measure of the bare bending rigidity, confirmed that the amphiphilic film is stiffened with increasing pressure.

Supercritical balanced CO_2-microemulsions are difficult to formulate and only a few compositions have been successful so far. They are similar to oil containing microemulsions with regard to structural and elastic properties. However, the ability to freely vary the density of $scCO_2$ and therewith its solvent quality allows fundamental aspects of the elastic properties of microemulsions to be studied at constant composition.

Acknowledgements

We wish to thank L. Kramer for his help in the early stages of these studies, O. Klems and V. Dahl for their assistance with the SANS experiments and Klaus Wormuth for his careful revision of the manuscript. Furthermore we would like to thank H. Metzner and the technical workshop as well as W. Röhl for their essential contributions in the development of the high-pressure cells. We also thank the Fund of the Chemical Industry in Germany (VCI), the International Helmholtz Research School of Biophysics and Soft Matter (IHRS BioSoft) as well as the EU-network of excellence SoftComp for financial support. In addition we wish to thank DuPont for the free Zonyl samples. Finally we thank the ILL and the JCNS for the opportunity to perform neutron scattering experiments and for financial support.

Notes and references

1 W. Jahn and R. Strey, *J. Phys. Chem.*, 1988, **92**, 2294–2301.
2 M. Kahlweit, R. Strey, R. Schomacker and D. Haase, *Langmuir*, 1989, **5**, 305–315.
3 B. Lindman, K. Shinoda, U. Olsson, D. Anderson, G. Karlstrom and H. Wennerstrom, *Colloids Surf.*, 1989, **38**, 205–224.
4 G. Gompper and M. Schick, in *Phase Transitions and Critical Phenomena*, ed. C. Domb and J. Lebowitz, Academic Press, London, 1994.
5 W. Helfrich, *Z. Naturforsch., C: Biochem., Biophys., Biol., Virol.*, 1973, **28**, 693.
6 P. Pieruschka, S. A. Safran and S. T. Marcelja, *Phys. Rev. E: Stat. Phys., Plasmas, Fluids, Relat. Interdiscip. Top.*, 1995, **52**, 1245–1247.
7 T. Sottmann and R. Strey, in *Fundamentals of Interface and Colloid Science*, ed. J. Lyklema, Elsevier Academic Press, Heidelberg, 2005.
8 H. Endo, J. Allgaier, G. Gompper, B. Jakobs, M. Monkenbusch, D. Richter, T. Sottmann and R. Strey, *Phys. Rev. Lett.*, 2000, **85**, 102–105.
9 H. Endo, M. Mihailescu, M. Monkenbusch, J. Allgaier, G. Gompper, D. Richter, B. Jakobs, T. Sottmann, R. Strey and I. Grillo, *J. Chem. Phys.*, 2001, **115**, 580–600.
10 B. Jakobs, T. Sottmann, R. Strey, J. Allgaier, L. Willner and D. Richter, *Langmuir*, 1999, **15**, 6707–6711.
11 M. Mihailescu, M. Monkenbusch, H. Endo, J. Allgaier, G. Gompper, J. Stellbrink, D. Richter, B. Jakobs, T. Sottmann and B. Farago, *J. Chem. Phys.*, 2001, **115**, 9563–9577.
12 D. Byelov, H. Frielinghaus, O. Holderer, J. Allgaier and D. Richter, *Langmuir*, 2004, **20**, 10433–10443.
13 A. Hanke, E. Eisenriegler and S. Dietrich, *Phys. Rev. E: Stat. Phys., Plasmas, Fluids, Relat. Interdiscip. Top.*, 1999, **59**, 6853–6878.
14 J. Eastoe and S. Gold, *Phys. Chem. Chem. Phys.*, 2005, **7**, 1352–1362.
15 J. Eastoe, S. Gold and D. C. Steytler, *Langmuir*, 2006, **22**, 9832–9842.
16 M. Schwan, L. G. A. Kramer, T. Sottmann and R. Strey, *Phys. Chem. Chem. Phys.*, 2010, **12**, 6247–6252.

17 K. Harrison, J. Goveas, K. P. Johnston and E. A. Orear, *Langmuir*, 1994, **10**, 3536–3541.
18 T. A. Hoefling, R. M. Enick and E. J. Beckman, *J. Phys. Chem.*, 1991, **95**, 7127–7129.
19 J. Eastoe, A. Paul, A. Downer, D. C. Steytler and E. Rumsey, *Langmuir*, 2002, **18**, 3014–3017.
20 S. Senapati, J. S. Keiper, J. M. DeSimone, G. D. Wignall, Y. B. Melnichenko, H. Frielinghaus and M. L. Berkowitz, *Langmuir*, 2002, **18**, 7371–7376.
21 M. Sagisaka, S. Yoda, Y. Takebayashi, K. Otake, B. Kitiyanan, Y. Kondo, N. Yoshino, K. Takebayashi, H. Sakai and M. Abe, *Langmuir*, 2003, **19**, 220–225.
22 A. Dupont, J. Eastoe and L. Martin, *Langmuir*, 2004, **20**, 9960–9967.
23 Y. N. Gao, W. Z. Wu, B. X. Han, G. Z. Li, J. W. Chen and W. G. Hou, *Fluid Phase Equilib.*, 2004, **226**, 301–305.
24 M. Klostermann, L. G. A. Kramer, T. Sottmann and R. Strey, *Langmuir*, 2010, in preparation.
25 O. Holderer, M. Klostermann, M. Monkenbusch, R. Schweins, P. Lindner, R. Strey, P. Richter and T. Sottmann, *Phys. Chem. Chem. Phys.*, 2011, **13**, 3022–3025.
26 M. Kahlweit, R. Strey, D. Haase, H. Kunieda, T. Schmeling, B. Faulhaber, M. Borkovec, H. F. Eicke, G. Busse, F. Eggers, T. Funck, H. Richmann, L. Magid, O. Soderman, P. Stilbs, J. Winkler, A. Dittrich and W. Jahn, *J. Colloid Interface Sci.*, 1987, **118**, 436–453.
27 M. Monkenbusch, R. Schatzler and D. Richter, *Nucl. Instrum. Methods Phys. Res., Sect. A*, 1997, **399**, 301–323.
28 O. Holderer, M. Monkenbusch, G. Borchert, C. Breunig and K. Zeitelhack, *Nucl. Instrum. Methods Phys. Res., Sect. A*, 2008, **586**, 90–94.
29 M. Teubner and R. Strey, *J. Chem. Phys.*, 1987, **87**, 3195–3200.
30 S. H. Chen, S. L. Chang and R. Strey, *Prog. Colloid Polym. Sci.*, 1990, **81**, 30–35, 302.
31 R. Strey, J. Winkler and L. Magid, *J. Phys. Chem.*, 1991, **95**, 7502–7507.
32 G. Porod, in *Small Angle X-Ray Scattering*, ed. O. Glatter and O. Kratky, Academic Press, New York, 1982.
33 A. G. Zilman and R. Granek, *Phys. Rev. Lett.*, 1996, **77**, 4788–4791.
34 T. Hellweg and D. Langevin, *Phys. A*, 1999, **264**, 370–387.
35 L. R. Arriaga, I. Lopez-Montero, F. Monroy, G. Orts-Gil, B. Farago and T. Hellweg, *Biophys. J.*, 2009, **96**, 3629–3637.
36 R. Strey, *Colloid Polym. Sci.*, 1994, **272**, 1005–1019.
37 S. H. Chen, S. L. Chang and R. Strey, *Prog. Colloid Polym. Sci.*, 1990, **81**, 30–35.
38 T. Sottmann, R. Strey and S. H. Chen, *J. Chem. Phys.*, 1997, **106**, 6483–6491.
39 L. Peliti and S. Leibler, *Phys. Rev. Lett.*, 1985, **54**, 1690–1693.
40 L. Golubovic, *Phys. Rev. E: Stat. Phys., Plasmas, Fluids, Relat. Interdiscip. Top.*, 1994, **50**, R2419–R2422.
41 D. C. Morse, *Phys. Rev. E: Stat. Phys., Plasmas, Fluids, Relat. Interdiscip. Top.*, 1994, **50**, R2423–R2426.
42 G. Gompper and D. M. Kroll, *Phys. Rev. Lett.*, 1998, **81**, 2284–2287.
43 O. Holderer, H. Frielinghaus, D. Byelov, M. Monkenbusch, J. Allgaier and D. Richter, *J. Chem. Phys.*, 2005, **122**, 094908.
44 B. Farago, M. Monkenbusch, K. D. Goecking, D. Richter and J. S. Huang, *Phys. B*, 1995, **213**, 712–717.
45 S. Komura, T. Takeda, Y. Kawabata, S. K. Ghosh, H. Seto and M. Nagao, *Phys. Rev. E: Stat., Nonlinear, Soft Matter Phys.*, 2001, **6304**.
46 P. Linder and R. Schweins, *Neutron News*, 2010, **21**(2), 15–18.